Available online at www.sciencedirect.com
ScienceDirect
Journal of Controlled Release 121 (2007) 100–109
journal of controlled release
www.elsevier.com/locate/jconrel

NanoCipro encapsulation in monodisperse large porous PLGA microparticles

Matthew M. Arnold [a], Eric M. Gorman [b], Loren J. Schieber [b], Eric J. Munson [b], Cory Berkland [a,b,*]

[a] Department of Chemical and Petroleum Engineering, The University of Kansas, Lawrence, KS 66047, United States
[b] Department of Pharmaceutical Chemistry, The University of Kansas, Lawrence, KS 66047, United States

Received 7 March 2007; accepted 30 May 2007
Available online 13 June 2007

Abstract

Pulmonary drug delivery of controlled release formulations may provide an effective adjunct approach to orally delivered antibiotics for clearing persistent lung infections. Dry powder formulations for this indication should possess characteristics including; effective deposition to infected lung compartments, persistence at the infection site, and steady release of antibiotic. Large porous particles (~10–15μm) have demonstrated effective lung deposition and enhanced lung residence as a result of their large diameter and reduced clearance by macrophages in comparison to small microparticles (~1–5μm). In this report, Precision Particle Fabrication technology was used to create monodisperse large porous particles of poly(D,L-lactic-co-glycolic acid) (PLGA) utilizing oils as extractable porogens. After extraction, the resulting large porous PLGA particles exhibited a low density and a web-like or hollow interior depending on porogen concentration and type, respectively. Ciprofloxacin nanoparticles (nanoCipro) created by homogenization in dichloromethane, possessed a polymorph with a decreased melting temperature. Encapsulating nanoCipro in large porous PLGA particles resulted in a steady release of ciprofloxacin that was extended for larger particle diameters and for the solid particle morphology in comparison to large porous particles. The encapsulation efficiency of nanoCipro was quite low and factors impacting the entrapment of nanoparticles during particle formation were elucidated. A dry powder formulation with the potential to control particle deposition and sustain release to the lung was developed and insight to improve nanoparticle encapsulation is discussed.
Published by Elsevier B.V.

Keywords: Microsphere; Nanoparticle; Controlled release; PLGA; Ciprofloxacin; Pulmonary; Aerosol

1. Introduction

Ciprofloxacin has been shown to be effective in treating several types of bacterial infections, in particular lung infections [1]. One of the major obstacles in using the drug to treat infections of the lung lies not in the efficacy of the drug, but in getting therapeutic quantities of the drug to the site of infection [2]. Oral antibiotics represent a commonly prescribed therapy and remain the most effective therapeutic approach; however, infections are often persistent and exceedingly difficult to clear [1]. For example, a current treatment regimen of cystic fibrosis entails oral administration of ciprofloxacin, an antibacterial chemotherapeutic, at a dose of 300mg administered on a twice-daily basis for alternating 28-day on–off cycles. Typically 0.5 to 5% of each dose enters the bloodstream and ~10 percent of circulating drug reaches the infection site [3]. The low efficacy may potentially be circumvented by applying the drug more directly to the site of infection, thus, suggesting an aerosol administered directly to the lung may improve therapeutic performance as compared to oral dosing and falling prey to first pass metabolism and dilution effects.

While the pulmonary route has distinct advantages over the oral route, a major drawback lies in the inability to consistently access the deep lung, where the seat of the infection usually lies. This severely limits the effectiveness of treatment, especially in the case of patients with lung infections that compromise tidal inhalation and total inhalation volume. In order to more fully capitalize on this drug delivery method, a need exists for a reliable way to deliver ciprofloxacin to all areas of the lung,

* Corresponding author. Department of Chemical and Petroleum Engineering, The University of Kansas, Lawrence, KS 66047, United States. Tel.: +1 785 864 1455; fax: +1 785 864 1454.
E-mail address: berkland@ku.edu (C. Berkland).

0168-3659/$ - see front matter. Published by Elsevier B.V.
doi:10.1016/j.jconrel.2007.05.039

especially the deep lung, to more fully treat and eradicate any and all infection. A sustained concentration of antibiotic delivered locally to the lung may further improve performance providing an adjunct therapy to current oral antibiotic delivery.

A large amount of work has been directed in the last 40years towards the development of polymeric microparticles as drug delivery vehicles [4]. Polymer chemistry and control over the particle size distribution through emulsification-type processes have been used, along with other factors, to control the release rate of the drug from the particles [5]. Much effort has been expended in predicting the loading and release of various drugs from polymeric microparticles [4]. In particular, modulating both the average size, size distribution, and the degradation rate of the microsphere allows control of the release kinetics, all other variables being the same [6–9]. A popular polymer used today is poly(D,L-lactic-co-glycolic acid) (PLGA), highly regarded for its safe biodegradability in the body and approval by the FDA. Preliminary evaluations of PLGA toxicology in the lung are promising, but work remains to prove this material for sustained pulmonary drug delivery [10,11].

Successful targeting of this controlled release polymer to specific areas of the lungs requires careful control over particle size. Researchers have found that ~1–3μm particles deposit with high efficiency to the deep lung and ~4–8μm particles to the bronchial region, whereas larger particles (>10μm) tend to be deposited along the oropharangyal cavity [12]. However, smaller particles tend to more easily agglomerate into larger particles potentially impacting aerosol performance. In addition, distributions that include a wide range of both large and small particle sizes have shown a lack of control in depositing the drug at the specific sites of infection [13]. To deal with these problems, recent work has focused on "large porous" particles exhibiting geometric diameters larger than 10μm but with aerodynamic diameters of ~1–3μm [14–17]. Large porous particles exhibit the aerodynamics of smaller particles while maintaining a size large enough to resist uptake by alveolar macrophages [18]; however, a narrow aerodynamic diameter is still desired. The aerodynamic diameter of a porous particle is given by Eq. (1), where d_{aero} stands for aerodynamic diameter, d_{geo} is the geometric particle diameter, γ is the shape factor (1 if the particle is a sphere), $\rho_{particle}$ is the particle density, and ρ_{ref} is a reference density.

$$d_{aero} = d_{geo}\left(\frac{\rho_{particle}}{\rho_{ref}\cdot\gamma}\right)^{1/2} \quad (1)$$

In this work, immiscible oil is added to PLGA dissolved in dichloromethane containing a nanosuspension of ciprofloxacin (abbreviated here as nanoCipro, ~400nm). Following the double emulsion, organic solvent is extracted to produce oil/PLGA/drug particles. The oil is then extracted to produce large porous particles. Monodisperse large porous particles were produced by using the reported Precision Particle Fabrication technique [7–9,19]. Porous microparticles exhibited discrete particle size in the range appropriate for pulmonary drug delivery. As a result, the porous particles maintained a narrow density distribution while demonstrating control of the density of particles over a range of discrete sizes. We examined two different types of oil, canola oil and silicon oil, to determine the effect of porogen on particle density and morphology. Experiments were also performed to determine the crystalline form of the nanoCipro. A series of release experiments demonstrated steady ciprofloxacin release behavior from monodisperse large porous particles, but more rapid release compared to traditional solid PLGA microspheres. Surprisingly, nanoCipro possessed a very low encapsulation efficiency despite its poor solubility in water (~75μg/mL) and processing fluids (dichloromethane and heptane). Finally, we address the phenomena of microencapsulation of nanoparticles with respect to droplet dynamics during particle formation as a rationale for the low encapsulation efficiency to provide insight to future researchers pursuing microencapsulation of nanoparticles.

2. Materials and methods

2.1. Materials

Poly(D,L-lactide-co-glycolide) (50:50 lactic acid:glycolic acid; i.v.=0.31dL/g; M_w ~31,000) was obtained from Absorbable Polymers, Inc. Poly(vinyl alcohol) (PVA; 88% hydrolyzed) was obtained from Polysciences, Inc. Ciprofloxacin was obtained from Sigma Aldrich. Commercial grade canola oil and silicon oil (viscosity=57cP and 100cP, respectively) were used as porogens. HPLC grade dichloromethane (DCM), dimethylsulfoxide, and heptane were from Fisher Scientific.

2.2. Preparation of microspheres and nanoCipro

Microspheres were prepared by first creating a solution of 0.5% to 5% (w/v) PLGA in DCM. Due to the low solubility of ciprofloxacin in DCM, a nanosuspension was obtained by sonicating the Ciprofloxacin/PLGA solution for 90s at the maximum microtip power (Fisher Scientific Sonic Dismembrator Model 500), producing a homogenous nanosuspension. In some cases, canola oil was added to the Cipro/PLGA nanosuspension and again sonicated at the maximum microtip power for 90s. This solution was then immediately transferred to the spray device, where it was pumped through a nozzle at flow rates ranging from 0.25 to 6.0mL/hr. A carrier stream (1% PVA in distilled water) was pumped at flow rates ranging from 0.4 to 4.0mL/min and surrounded the emerging polymer stream and pulled it through a concentric, outer glass nozzle. Concurrently, an ultrasonic transducer (Branson Ultrasonics) controlled by a frequency generator (Hewlett Packard model 3325A) disrupted the emerging polymer jet into uniform droplets. For more details on this Precision Particle Fabrication technology, please see references [7–9,19–22]. The streams flowed into a beaker containing approximately 200–300mL of 1% PVA, and the particles were stirred at room temperature for three hours, filtered, and rinsed with distilled water. The particles were then washed with heptane (~30–40mL) to extract the canola or silicon oil when included, and rinsed again with deionized water (~150–200mL) to flush away any remaining heptane. The microspheres were lyophilized (Labconco benchtop model) for a minimum of 48h and stored at −20°C under desiccant.

2.3. Particle size distribution

NanoCipro size was determined using a Brookhaven ZetaPALS system. A Coulter Multisizer 3 (Beckman Coulter Inc.) equipped with a 50-μm or 100-μm aperture was used to determine the geometric size distribution of the various particle preparations. The lyophilized particles were resuspended in Isoton electrolyte, and at least 5000 microspheres were analyzed for each sample. The aerodynamic size distribution of lyophilized particles was determined with an Aerosizer LD (Amherst Instruments). The instrument used a pair of lasers to determine the time-of-flight for a population of particles, and fit a normal distribution to this data. About 2mg of sample was analyzed through a 700μm nozzle and a maximum shear rate of 5.0psi. Time-of-flight measurements should be interpreted in light of published data, which revealed significant error for particles with densities deviating from unity ($1 g/cm^3$) and for particles with aerodynamic diameters >10μm [23].

2.4. Microscopy

Microsphere surface structure and porosity were investigated by scanning electron microscopy (LEO Field Emission Scanning Electron Microscopy). Samples were prepared by placing a droplet of an aqueous microsphere suspension onto a silicon stub. The samples were dried overnight and were sputter coated with gold prior to imaging at 2–10eV. Particle cross-sections were attained by first cryofracturing the particles before preparing the silicon stub. Particles on a microscope slide were positioned above a shallow bowl filled with liquid nitrogen and chopped with a razor blade. Laser scanning confocal microscopy allowed the detection of ciprofloxacin within microparticles by using the 458nm line of a Zeiss Meta 510 and imaged at 468nm.

2.5. Thermal analysis

Differential scanning calorimetry (DSC) curves were collected on a Q100 DSC from TA Instruments using crimped aluminum pans containing 1.5–4mg of sample. Unless indicated, all DSC curves were collected from −80°C to 400°C with a heating rate of 20°C/min. under dry nitrogen. Thermogravimetric analysis (TGA) was performed using a Q50 TGA from TA Instruments. A platinum sample pan was loaded with ~3mg of sample and heated from ~20°C to 400°C at a rate of 20°C/min under dry nitrogen. Data analysis was completed using Universal Analysis 2000 (Version 4.3A) software that was provided by TA Instruments.

2.6. Solid-state NMR spectroscopy

All ^{13}C spectra were collected using a Chemagnetics CMX-300 spectrometer using variable amplitude cross-polarization (VACP) [24], magic-angle spinning (MAS) [25], and two pulse phase modulation (TPPM) decoupling [26]. Samples were packed into 7mm o.d. zirconia rotors and held in the rotors by Teflon® endcaps. The samples were spun at ~7.5kHz in 7mm spin modules from Revolution NMR (Fort Collins, CO). The spectrum of the as received ciprofloxacin is the sum of 2,048 transients collected using an 8s pulse delay and a contact time of 2ms. The nanoCipro batch #1 spectrum is the sum of 23,000 transients with a pulse delay of 2s and a contact time of 1.5ms. The nanoCipro batch #2 spectrum is the sum of 14,000 transients with a pulse delay of 4s and a contact time of 1.5ms. All of the spectra were collected with a ^1H 90° pulse width of 3.7μs. The free induction decays consisted of 1024 data points with a dwell time of 33.3μs. The spectra were externally referenced to tetramethylsilane using the methyl peak of 3-methylglutaric acid at 18.84ppm [27].

All ^{19}F spectra were collected using a Tecmag Apollo spectrometer operating at 284.1MHz using ramped amplitude cross-polarization (RAMP) [28], MAS [25], and TPPM decoupling [26]. Samples were packed into 3.2mm o.d. zirconia rotors and held in the rotors by Torlon® endcaps. The samples were spun at 21kHz in 3.2mm spin modules from Varian (Palo Alto, CA). The spectrum of the as received ciprofloxacin is the sum of 256 transients collected using a 15s pulse delay. The nanoCipro batch #1 spectrum is the sum of 1024 transients with a pulse delay of 2s. Both spectra were acquired with a contact time of 3ms and a ^1H 90° pulse width of 3μs. The free induction decays consisted of 1024 data points with a dwell time of 10μs. The spectra were externally referenced to Teflon® at −121.0ppm.

2.7. Determination of drug loading

The initial loading of ciprofloxacin was determined by dissolving a known mass (~10mg) of microspheres in 1.5mL of 70:30 dimethylsulfoxide:deionized water. Ciprofloxacin concentration in the solution was determined by measuring the absorbance at 320nm in a spectrophotometer (Agilent Technologies #8453). PLGA particles were used as blanks.

2.8. Drug release studies

Ciprofloxacin release was determined by resuspending a known mass of microspheres encapsulating ciprofloxacin in 1.6mL of phosphate buffered saline (PBS, pH 7.4). The suspensions were continuously agitated in an incubator/shaker (New Brunswick C24) at 50rpm and 37°C. At regular intervals the samples were centrifuged, the supernatant was removed, and the microspheres were resuspended in fresh PBS. The concentration of ciprofloxacin in the supernatant was determined using the UV detection method described above. The absorption of supernatant collected from blank PLGA particles showed a negligible absorption at 320nm throughout the release study. The amount of ciprofloxacin in each sample was summed with the amounts at each previous time point, and the total divided by the amount of ciprofloxacin in the microspheres (experimental loading times mass of microspheres) to calculate the cumulative percent released.

2.9. Statistics

Significant differences were calculated using a paired Student's *t*-test. Values of $p<0.05$ were considered significant.

3. Results

3.1. Variations in microparticle aerodynamics depends on porogen type and percentage

Solid PLGA microspheres containing nanoCipro were fabricated with average dry geometric diameters of 5.1, 7.2, and 20μm, as determined by measurement of SEM images (Table 1). Large porous particles were fabricated by following the same procedure, but including canola or silicon oil as part of the sonicated polymer solution. Oils were extracted by rinsing the particles with heptane after extraction of DCM. Large porous particles using a canola oil porogen possessed dry geometric diameters of 4.7, 7.7, 11, and 25μm. Sizes were purposefully generated with geometric and aerodynamic diameters that closely correspond to the geometric diameters of solid microspheres. These particles were utilized in ciprofloxacin release studies in comparison to solid particles. The wet particle size, determined by a Coulter Multisizer III, was divided by the diameter of the dry particles to calculate the microparticle swelling ratio. The diameter of hydrated particles was always greater than the diameter of dry particles as expected; however, no clear trend existed between the amount or type of porogen employed and the swelling ratio.

The aerodynamic diameters of lyophilized PLGA microparticle formulations containing nanoCipro were determined using an Aerosizer LD. The average aerodynamic diameter was divided by the dry geometric diameter for formulations as a method to calculate the relative density of the dry powders. The absolute density of PLGA, 1.34g/cm^3, was determined using a helium pyncnometer and used as the reference density for relative density calculations. The ratio of the aerodynamic diameter to geometric diameter ranged from 0.95 to 0.98 for solid PLGA microspheres containing nanoCipro, which corresponded to a density range of 1.21 to 1.29g/cm^3, where the density is determined by back-calculating from Eq. (1). These values are not significantly different than the density value of the PLGA used in calculations. Uniform porous microparticles made using an oil to PLGA ratio of 0.87 produced large porous particles with calculated densities of 0.95 to 1.11g/cm^3. In contrast to the solid PLGA microspheres, these values show a significant difference from the density of the PLGA ($p<0.05$) and from solid microspheres ($p<0.02$). Increasing the oil to PLGA ratio resulted in a corresponding decrease in particle density. Large porous particles fabricated using silicon oil as the porogen reflected similar particle properties in comparison to the corresponding particles using canola oil as the porogen.

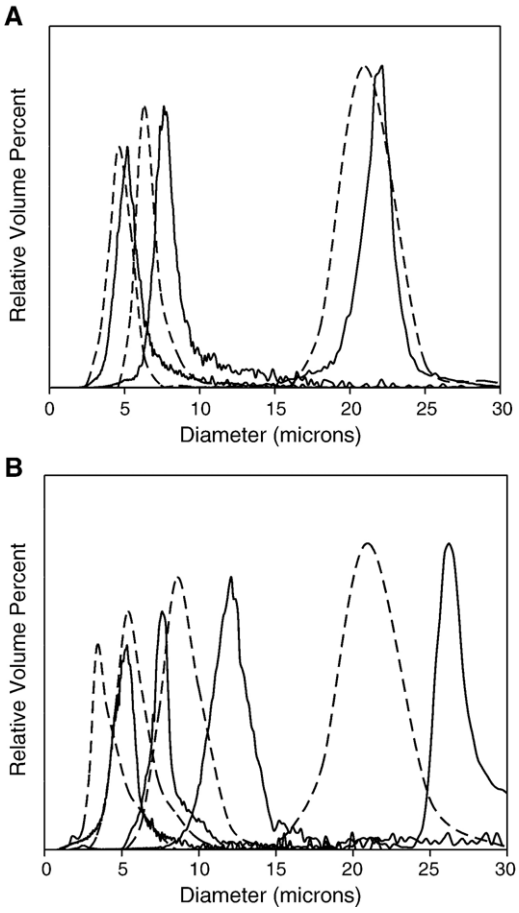

Fig. 1. Size distributions for (A) solid and (B) porous microparticles. Peak heights are equal for corresponding geometric (solid lines) and aerodynamic (dashed lines) distributions, with the aerodynamic diameter always smaller than the geometric.

The geometric size distributions (Coulter Multisizer III) and corresponding aerodynamic size distributions (Aerosizer LD) were quite narrow (Fig. 1). For the solid particle size

Table 1
PLGA microparticle formulations

Particle type	Solid	Solid	Solid	Porous	Porous	Porous	Porous	Porous	Porous	Porous	Porous
Porogen used	None	None	None	Canola	Canola	Canola	Canola	Canola	Canola	Silicon	Silicon
Oil wt./PLGA wt.	0	0	0	0.87	0.87	0.87	0.87	1.88	3.58	0.87	0.98
d_{geo} dry (μm)	5.1±0.3	7.2±0.2	20±0.2	4.7±0.2	7.7±0.4	11±0.3	25±0.2	9.6±0.3	15±0.3	27±0.2	16±0.5
d_{geo} wet (μm)	5.6±0.3	8.0±0.2	21±0.0	5.7±0.3	8.3±0.2	12±0.2	28±0.1	12±0.2	18±0.1	31±0.1	18±0.2
Swelling ratio [a]	1.09	1.10	1.06	1.19	1.08	1.11	1.12	1.28	1.19	1.14	1.12
d_{aero} (μm)	4.8±0.2	6.9±0.2	20±0.1	4.0±0.4	6.4±0.2	9.9±0.2	22±0.1	5.2±0.3	6.5±0.3	23±0.1	14±0.2
d_{aero}/d_{geo} [b]	0.95	0.96	0.98	0.85	0.84	0.91	0.90	0.55	0.43	0.86	0.84
$\rho_{particle}/\rho_{PLGA}$ [c]	0.90	0.92	0.96	0.72	0.71	0.83	0.81	0.30	0.18	0.74	0.71
$\rho_{particle}$ [c]	1.21	1.23	1.29	0.96	0.95	1.11	1.09	0.41	0.24	0.99	0.95

[a] Averaged value of d_{geo} wet/d_{geo} dry.
[b] Averaged value of d_{aero}/d_{geo} dry.
[c] Averaged value −1.34 g/cm^3 used for PLGA density and $\gamma=1$ used in calculations.

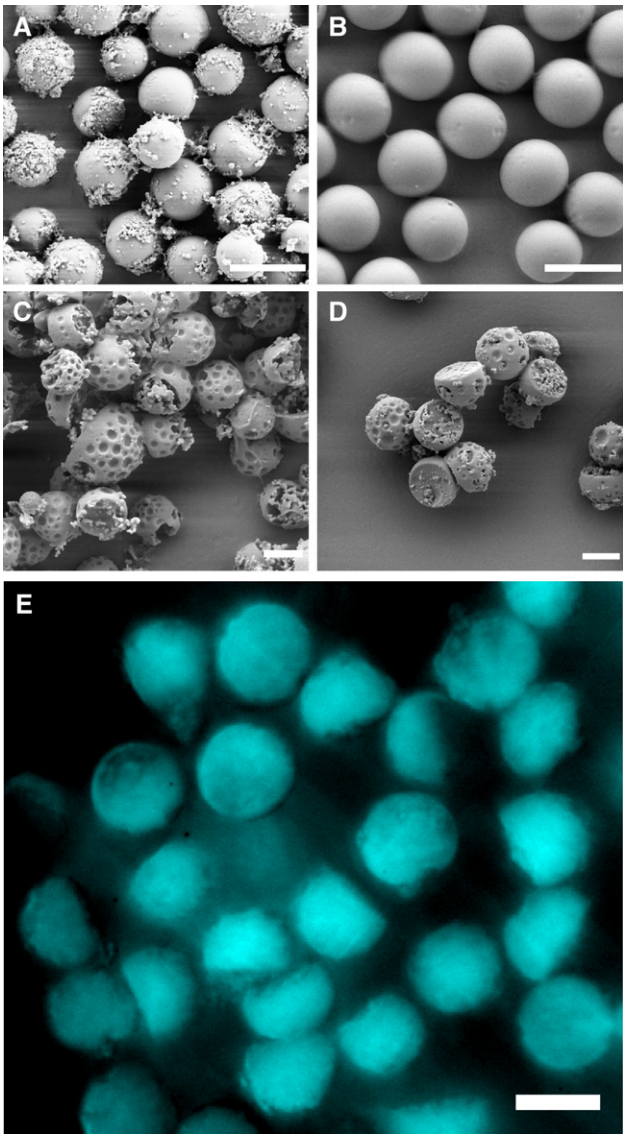

Fig. 2. Scanning electron micrographs of the surface morphology of solid (A) 7.2 μm and (B) 20 μm and porous (C) 7.7 μm and (D) 11 μm (bottom) microparticles. Scale bars = 10 μm. (E) Laser scanning confocal microscopy was used to detect the distribution of ciprofloxacin within large porous microparticles (0.87 Oil wt:PLGA wt). Scale bar = 10 μm.

distributions, the two graphs do not completely overlap; the average aerodynamic diameter is always slightly smaller than the average geometric diameter. This result occurred due to the swelling of the hydrated PLGA particles used for determining geometric size distributions in comparison to the dry particles used to determine the aerodynamic size distribution. On the other hand, particles employing 0.87 canola oil:PLGA ratio demonstrated distinctly shifted aerodynamic size distributions. The slight shoulder appearing on the smallest particle distribution (4μm aerodynamic diameter) may be indicative of some particle agglomeration in the aerosolized dry powder.

3.2. Particle morphology was influenced by porogen

The particle morphology exhibited a dimpled, closed-pore structure for the porous particles formed using canola oil as the porogen in contrast to the relatively smooth surface of the solid particles (Fig. 2). Surface pockmarks presumably formed when pockets of oil on the surface of the PLGA particle were washed away. The irregular surface may have been a primary reason for the limited amount of particle agglomeration observed in particle aerodynamic size distributions of dried powders by inhibiting particles from orderly packing. Packing inhibition may also be enhanced by the flat face present on most of the porous particles made using the canola oil porogen, which formed when a hemispherical section of oil making up part of the spherical droplet was later extracted. A high degree of control over particle size was also evident in electron micrographs. NanoCipro was also observed as clusters of smaller particles (~400nm) that clumped together on the surface of many of the PLGA particles; however, laser scanning confocal microscopy revealed that ciprofloxacin was distributed evenly throughout the particle matrix (Fig. 2E).

When silicon oil was used as the porogen, particle morphology noticeably changed. While canola oil led to particles formed with a porous, web-like internal structure, using silicon oil formed hollow particles (Fig. 3). In addition, particles containing silicon oil did not form the flat face evident in particles fabricated using canola oil as the porogen. The surfaces of the two types of particles exhibited a similar pockmarking effect

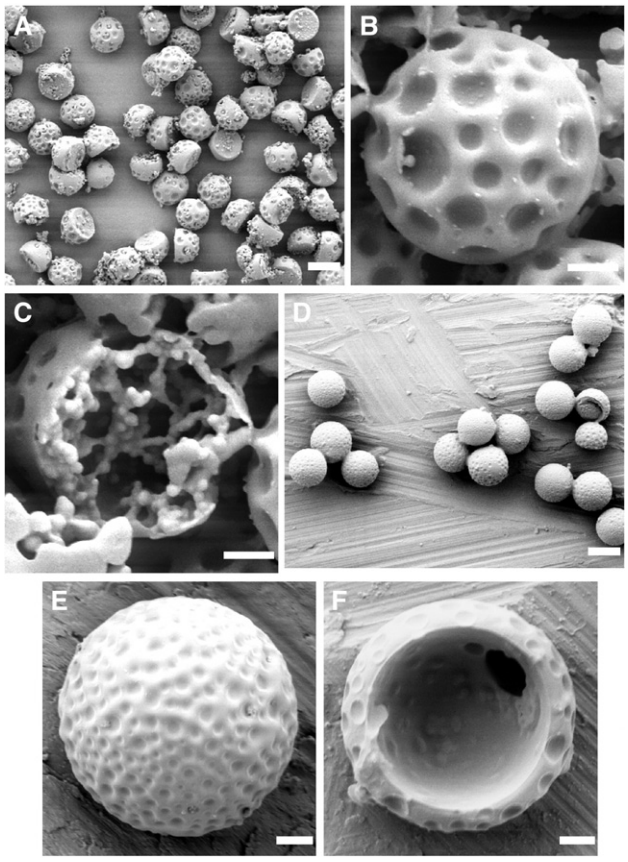

Fig. 3. Scanning electron micrographs of large porous particles using canola oil as a porogen depict the (A) bulk powder, (B) surface morphology, and (C) interior morphology. Similar micrographs of large porous particles using silicon oil as a porogen depict the (D) bulk powder, (E) surface morphology, and (F) interior morphology. Scale bar = 10 μm for A, D and 2 μm for B, C, E, F.

with dimples that covered the surface. Despite the differences in morphology, the porous particles made with silicon oil exhibited similar aerodynamic properties to those made with canola oil, having a density that closely corresponded to those previously fabricated with canola oil at the same ratio (Table 1). It is worth noting that nanoCipro particles were evident within the internal structure and embedded on the surface of PLGA particles using canola oil porogen (Fig. 3). Particles using silicon oil were not formulated with nanoCipro.

3.3. NanoCipro processing resulted in a polymorphic change

The DSC curve of the ciprofloxacin, as it was received from Sigma Aldrich Chemicals, exhibits a strong endothermic event at 271°C (Fig. 4A). TGA was performed on the material, and a large mass loss was observed at the same temperature (data not shown). The effect of heating rate on this transition was then observed using DSC by heating the material at different heating rates (3, 10, and 20°C/min.). These experiments (data not shown) revealed that the onset temperature of this transition did not change, thus indicating that the material melts at 271°C and then immediately begins to degrade. The nanoCipro exhibits a second endotherm that begins at ~115°C (Fig. 4A). No mass loss is observed from the nanoCipro near 115°C by TGA (data not shown), indicating that the endotherm is not due to solvent loss. Therefore, this endotherm likely corresponds to a different

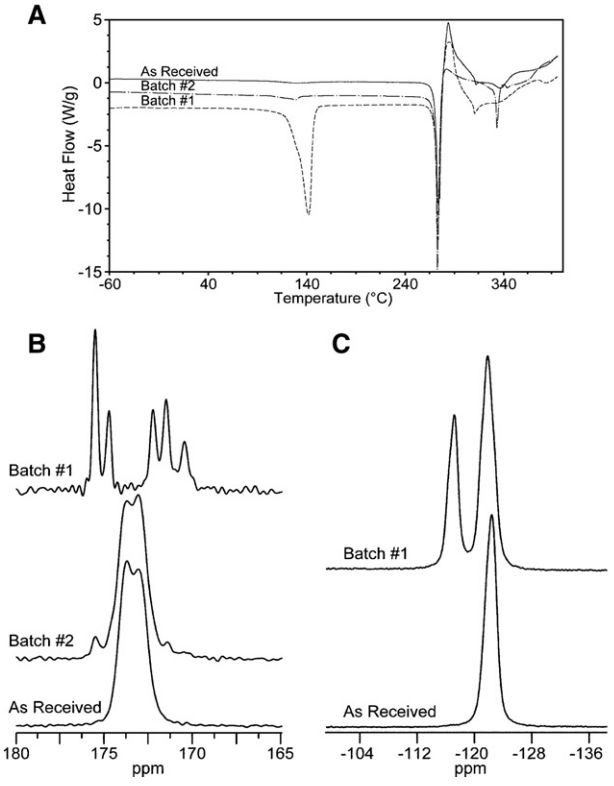

Fig. 4. (A) DSC curve of ciprofloxacin as received (solid line), nanoCipro batch #1 (dashed line), and nanoCipro batch #2 (dash dot) (exotherms are up). (B) ^{13}C CPMAS NMR spectra, and (C) ^{19}F CPMAS NMR spectra of ciprofloxacin as received and nanoCipro batch #1 and #2. ^{13}C CPMAS NMR spectra have been expanded to show only the carbonyl carbon peaks of ciprofloxacin.

Table 2
NanoCipro loading data for solid and porous microparticles

Particle type	Geometric diameter (μm)	Theoretical loading	Experimental loading	Encapsulation efficiency
Porous	5.7	4.49%	0.40%±0.13%	8.91%±2.90%
	8.3	3.95%	0.12%±0.04%	2.91%±1.01%
	12	4.84%	0.17%±0.05%	3.51%±1.03%
	28	8.92%	0.12%±0.01%	1.35%±0.11%
Solid	5.6	4.92%	0.18%±0.08%	3.66%±1.63%
	8.0	4.08%	0.08%±0.04%	1.96%±0.98%
	21	4.92%	0.13%±0.03%	2.54%±0.61%

polymorph. The polymorph that melts at 271°C is referred to as Form I and this new polymorph that has been observed in the nanoCipro is called Form II. The two batches of nanoCipro appear to contain different amounts of the Form II polymorph, with the first batch containing much more Form II than the second batch based on the size of the endotherm at ~115°C, even though processing conditions were identical.

The ^{13}C CPMAS NMR spectrum of the as received ciprofloxacin exhibits two overlapping peaks at 173 and 174ppm (Fig. 4B) that correspond to the carbonyl carbons of ciprofloxacin Form I. The first batch of the nanoCipro exhibits five peaks in this same region (Fig. 4A), none of which correspond to the two peaks in the original material. The peak splitting indicates that Form II likely has two molecules in the asymmetric unit of the crystallographic unit cell; thereby, each of the carbonyl carbons results in two peaks, yielding four peaks total. The extra peak at ~170ppm is likely due to an impurity; however, this was not confirmed. Additionally, the two peaks corresponding to Form I were not observed in this batch, indicating that the first batch was entirely Form II. When the second batch of nanoCipro is examined, the two peaks corresponding to Form I are clearly present and dominate the carbonyl region (Fig. 4B); however, the Form II peaks remain visible indicating that the second batch is primarily Form I but does contain some Form II.

The ^{19}F CPMAS data support the conclusions from the ^{13}C spectra. Ciprofloxacin contains only one F atom, thus, the ^{19}F CPMAS NMR spectrum should contain only one peak. For the as received ciprofloxacin, there is only one peak, as expected (Fig. 4C). On the other hand the first batch of nanoCipro displays two peaks (Fig. 4C), neither of which correspond to the peak in the as received material providing additional evidence that nanoCipro contains a new polymorph whose crystallographic unit cell contains two molecules per asymmetric unit. It is noteworthy that after a few months under ambient conditions the peaks corresponding to Form II had disappeared in the ^{19}F spectra of the nanoCipro and a peak corresponding to Form I had appeared, indicating that Form II is only moderately stable at room temperature.

A very small peak at ~−117ppm was observed in the ^{19}F spectrum for the as received ciprofloxacin. This might indicate the presence of an impurity or a small amount of Form II, as the downfield peak of Form II also occurs at approximately the same chemical shift. Closer examination of the DSC curve for the as received ciprofloxacin revealed a very small endotherm

centered around 130°C. Additionally, there appears to be small peaks on either side of the Form I peaks in the ^{13}C CPMAS spectrum of the as received material in approximately the same positions as the Form II peaks; however, the signal-to-noise ratio is not sufficient to definitively state that they truly are peaks and that they correspond to Form II. When taken together, all of this evidence appears to indicate that there might in fact be a very small amount of the Form II polymorph present in the ciprofloxacin as it was received.

3.4. Ciprofloxacin release depends on particle structure and size

NanoCipro was encapsulated into solid and porous microspheres using the 0.87 canola oil/PLGA ratio. Large porous microparticles observed by laser scanning confocal microscopy confirmed that the ciprofloxacin distribution was uniform throughout the particle matrix (data not shown). In addition, the diffuse fluorescence may indicate the presence of molecular ciprofloxacin as well as the nanoCipro particles. While a theoretical loading of 4–5% nanoCipro was targeted, the actual drug loading ranged from 0.08% to 0.4%, yielding alarmingly low encapsulation efficiencies (Table 2). The nanoCipro particles were fairly large with respect to the structure of the microparticles. The rationale for the low encapsulation efficiency based on fundamental mass transport theory as applied to microdroplet dynamics encapsulating nanoparticles is presented in the discussion section.

The results of the drug release experiment demonstrated a distinction between the ciprofloxacin release kinetics from solid and porous particles (Fig. 5). Generally, for a given particle size, the porous microparticles released at a faster rate than their solid equivalent, most likely due to the decreased resistance to the effective diffusion of solubilized ciprofloxacin. For both types of particles, the release rate increased as particle size decreased. The duration of unencapsulated nanoCipro dissolution was ~5days, which was extended to 2–4weeks depending on the microparticle size and structure. The release kinetics from both solid and porous microparticles generally followed similar trends suggesting that the release of ciprofloxacin may be attributable to nanoCipro dissolution coupled with the effective diffusion of ciprofloxacin through the degrading polymer matrix.

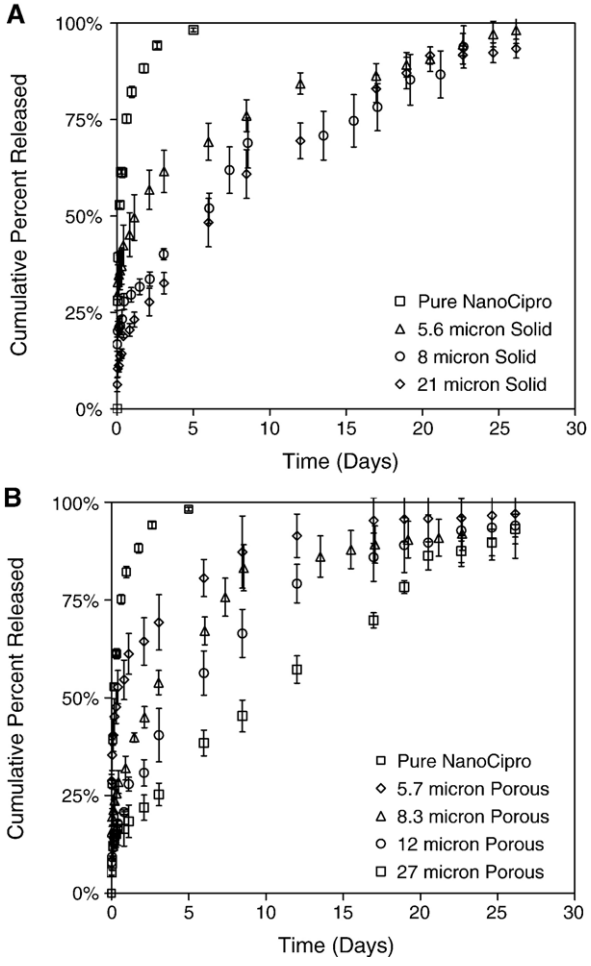

Fig. 5. Release kinetics of encapsulated nanoCipro from (A) solid microparticles and from (B) porous microparticles made using canola oil as a porogen (0.87 Oil wt.:PLGA wt.).

4. Discussion

4.1. Polymorphic changes in nanoCipro particles

Polymorphic changes can have a significant effect upon bioavailability; for example, when there exists a significant difference in the solubility of the different crystalline forms. Evidence from DSC and solid-state NMR showed that ciprofloxacin changes form upon sonication. Because ciprofloxacin is essentially insoluble in dichloromethane it is extremely unlikely that the form change occurred via a solvent-mediated polymorphic transformation because it was in contact with the dichloromethane for a relatively short time. It is also unlikely that the crystallites were dissolving and then recrystallizing because these would alter particle size. The most likely source for the transformation is the sonication process, where the shear forces may be responsible for the change in form. Although it was not investigated further, the Form II produced during the sonication process may have been incorporated into the microparticles, and subsequently undergone a polymorphic change during storage. Because of the relatively low drug loading, it is expected to be difficult to characterize the form of the nanoCipro in the microparticles.

4.2. Droplet dynamics and particle formation

The major focus of this work was to understand porogen effect on particle aerodynamics and ciprofloxacin release. To better understand particle performance, particle formation is discussed, including porogen and nanoCipro distribution in a droplet during solvent extraction. Using this 'oil and solid'-in-oil-in-water double emulsion/solvent extraction method, a finite amount of time exists for the oil or the nanoCipro suspension to maneuver within the droplet (Fig. 6). PLGA viscosity within the droplet increases (due to dichloromethane extraction) with time and oil and drug mobility correspondingly decrease. Later, oil is

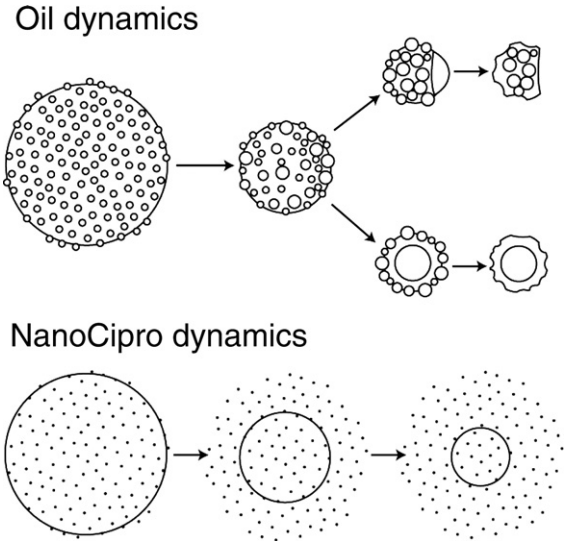

Fig. 6. Schematic representation of droplet dynamics during the formation process of large porous PLGA particles using an oil porogen (top) and solid PLGA particles encapsulating nanoCipro (bottom). As dichloromethane is extracted from the droplet, the diameter decreases. Oil porogen partitions within the droplet leading to surface pockmarks, a flat face, or a core. Exclusion of nanoCipro from the shrinking droplet provides one possible explanation of the low encapsulation efficiency.

extracted leaving a porous structure with a fraction of the drug trapped inside the polymeric particle. Envisioning the nascent droplet as a fluid, three-dimensional structure during the particle formation phase, altogether there are five different species to account for: PLGA, dichloromethane, aqueous surfactant solution, oil, and drug (nanoCipro, assuming only a small percentage of drug exists in solution). When the dichloromethane is extracted into the aqueous phase, the boundary of the droplet shrinks rapidly at first, then progressively slower [29]. As the dichloromethane is extracted its concentration within the droplet decreases until eventually the polymer precipitates out of solution and a hardened particle forms. Here, we examine the first stage of particle development, which comprises the formation of the spherical droplet in the surfactant solution to the point at which PLGA begins to precipitate out of solution (~10wt% dichloromethane) [29]. The second stage of particle development may be considered when the structure of the particle begins to take discrete shape until the final particle structure is achieved; here the mass transfer of species across the particle/aqueous solution interface has dropped to negligible levels.

The quantity dr / dt or v_r is important when assessing the effects of oil and nanoCipro dynamics on the porosity and drug encapsulation efficiency of the particle, respectively. Differentiating the droplet radius with respect to time gives the boundary velocity, and likewise this velocity sets the pace by which all other species in solution are referenced. Rapid movement of this boundary (convection) may dominate the mass transport of slowly diffusing materials (*e.g.* large polymers or nanoparticles). DeLucca and others state that 90% of dichloromethane can be removed from a dispersed droplet phase in <40s for low dichloromethane:water ratios (<1:100) [29], suggesting a very high extraction rate for experiments reported here, which employ a slow addition rate of dichloromethane and a large excess of water (>1:100). In other words, convective transport is expected to dominate diffusive transport of oil droplets or nanoCipro within nascent droplets.

4.3. Dynamics of oil distribution in a forming particle

Pock marks on the PLGA particle surface and the continuous web-like internal morphology when using the canola oil porogen (Figs. 3 and 4) suggest that the canola oil had a similar affinity for the aqueous extraction phase as PLGA. The thermodynamics of this phenomena, which considers interfacial tension effects on spreading coefficients, have been addressed thoroughly in the context of microencapsulation by Mathiowitz et al. [30,31] as well as in other previous reports [20,32]. The two competing effects are the rate at which the boundary is moving (convection), and the rate at which the oil is diffusing through the medium. The effective diffusion of oil would be hindered as the droplet viscosity increases during dichloromethane extraction. The pock marks on the surface of all of the particles may suggest that the movement of the oil was typically slower than the rate of the moving boundary [34]. The dimensionless number for comparing convective versus diffusive transport is the Peclet number (Eq. (2)), which is simply the product of the Reynolds number and the Schmidt number. Here, D is the droplet diameter, v_r is the boundary velocity, υ is the kinematic viscosity (μ/ρ), and D_A is the diffusion coefficient.

$$\mathrm{Re} = Dv_r/\upsilon \quad \mathrm{Sc} = \upsilon/D_A$$
$$\mathrm{Pe} = \mathrm{ReSc} = \left(\frac{Dv_r}{\upsilon}\right)\left(\frac{\upsilon}{D_A}\right) = \frac{Dv_r}{D_A} \tag{2}$$

The composition of the final particles suggests a high Peclet number. Given that the diffusional rate of a droplet of oil in the solution would not be more than 10^{-6}cm^2/s (initially, based on estimated oil droplet diameter greater than several hundred nanometers), and the velocity of the boundary is estimated to be on the order of 10^2μm/s (initially) [29], this gives a Peclet number on the order of 10^2 (~100μm droplet). Therefore, rapid movement of the boundary led to a pile-up of oil at the interface, which produced pock marks and a flat face upon extraction (Fig. 6). In the case of silicon oil, which possessed a lower density and viscosity than the canola oil, a distinct core of silicon oil produced a core/shell microparticle upon oil extraction. Despite the driving force for silicon oil/PLGA phase separation into a core/shell morphology during solvent extraction, the same pock marks were evident on the microparticle surface, again indicating that rapid boundary motion lead to oil droplets at the interface, despite interfacial tension driving the silicon oil to the droplet core.

4.4. Dynamics of nanoCipro distribution in a forming particle

A similar rationale can be extended to explain the low encapsulation efficiency of the nanoCipro. Here, we assume

that most of the drug is present in the nanoparticle form. Again, the drug nanoparticles are finely dispersed throughout the volume of the forming droplet and again, the two major competing effects are the diffusional rate of the drug and its net movement through the fluid versus the moving boundary of the droplet (Fig. 6). Given that ciprofloxacin is a zwitterionic drug, it exhibits a poor solubility in both the aqueous (neutral pH) and most organic phases. Since the drug does not exhibit substantial solubility in either phase, it would seem reasonable to assume that the driving force for the diffusion of the nanoCipro would be the concentration gradient between the droplet and the surrounding aqueous medium, independent of partitioning or dissolution effects. The diffusivity of the nanoCipro can be estimated by applying the Stokes–Einstein equation (Eq. (3)) [33]. Here, D_{AB} is the diffusion coefficient of nanoCipro in dichloromethane, k is Boltzmann's constant, T is temperature, μ is the viscosity of PLGA/dichloromethane (approximated as dichloromethane initially), and r_A is the radius of nanoCipro.

$$D_{AB} = \frac{kT}{6\pi\mu r_A} \tag{3}$$

The viscosity of the droplet solution changes based on the mass fraction of dichloromethane, so the diffusivity will likewise be dynamically dependant on the mass fraction of dichloromethane. The diffusional rate of the nanoCipro in the droplet solution has a maximum on the order of 10^{-5}cm^2/s (initially). The velocity of the boundary is again estimated to be on the order of 10^2μm/s (initially). Contrary to the description of oil "pile-up" at the droplet interface, rapid movement of the boundary led to passage of nanoCipro through the interface. This phenomena is further enlightened when considering polymer/solvent wettability of oil droplets in comparison to nanoCipro, which would not be preferentially wetted by the polymer/solvent due to the zwitterionic nature of the drug.

We have considered several explanations of the low nanoCipro encapsulation efficiency within a PLGA particle. Of course, the simplest explanation is dissolution of nanoCipro in the extraction media and/or loss during porogen extraction (ciprofloxacin logP ~1.3). Although this likely accounts for some percentage of the ciprofloxacin loss, drug dissolution (occurring on the order of hours to days) is much slower than PLGA particle formation. Since convection dominates, an estimation of nanoCipro encapsulation efficiency may simply assume that the nanoCipro particles remained stationary throughout the extraction process, fixed at their spatial location, while the droplet boundary moved inward. In this calculation, the mass of the nanoCipro inside the particle is simply the mass of the nanoCipro located inside the moving droplet diameter at a given time. In the case of a 10wt.% PLGA/vol. dichloromethane solution, we observed the final particle size was ~30% of the original droplet diameter, which translates into a particle that occupies only ~2.7% of the original droplet volume. Of course the concentration of PLGA greatly affects the solvent extraction kinetics of the forming particle as well as the final particle size [29]. Encapsulation efficiency calculated via this "volume exclusion" approach is in close agreement with the experimental values and emphasizes the likely mechanism of the strikingly low encapsulation efficiency observed. Improving nanoparticle encapsulation efficiency will require similar approaches to those used for drug molecules. Although direct conjugation of nanoparticles to PLGA is unlikely, one may be able to improve nanoparticle affinity for the organic phase by utilizing appropriate coating materials. A large amount of effort has focused on treating nanoparticles with hydrophilic surfaces; however, the opposite may be desired for enhancing encapsulation into relatively hydrophobic polymers. The desired result of surface modification would be preferential polymer/solvent wetting of the nanoparticles to encourage retention in the polymer matrix. Finally, encapsulation may be improved by decreasing nanoparticle mobility by increasing the initial polymer concentration.

5. Conclusions

Pulmonary infections are often persistent and recurrent due to the compromised nature of the pulmonary bed. A potential therapeutic approach is to sustain the delivery of antibiotics directly to the site of infection as a mechanism to increase and maintain the local drug concentration; however, accessing the deepest portions of the lung remains difficult. Dry powder aerosol formulations utilizing monodisperse large porous PLGA microparticles as carriers may address these encumbrances in multiple ways, although thorough toxicological studies of this polymer are still needed. Tight control over the geometric size and morphology of large porous particles resulted in aerosols with narrow aerodynamic size distributions. In addition, encapsulation of a nanosuspension of ciprofloxacin facilitated controlled release for 2–4weeks, a time frame suitable for avoiding antibiotic resistance assuming large porous particles persist in the lung [34]. Finally, the poor encapsulation efficiency of nanoparticles using a solvent extraction technique was addressed by modeling droplet dynamics during particle formation. Faced with a quickly moving boundary, a drastic change in volume, and a net flux away from the droplet center, nanoCipro had little opportunity to remain in the forming particle; however, a careful consideration of variables affecting particle formation should provide insight for future studies utilizing microencapsulated nanoparticles.

Acknowledgements

We are indebted to the PhRMA Foundation for supporting this work. The Microscopy Lab has our gratitude for assistance with imaging. EMG was supported by a Biotechnology Training Grant (NIH 29488) from the National Institute of General Medical Sciences.

References

[1] D.M. Wood, A.R. Smyth, Antibiotic strategies for eradicating *Pseudomonas aeruginosa* in people with cystic fibrosis, Cochrane Database Syst. Rev. (1) (2006) CD004197.

[2] S.A. Shoyele, A. Slowey, Prospects of formulating proteins/peptides as aerosols for pulmonary drug delivery, Int. J. Pharm. 314 (1) (2006) 1–8.

[3] H. Peltola, P. Ukkonen, H. Saxen, H. Stass, Single-dose and steady-state pharmacokinetics of a new oral suspension of ciprofloxacin in children, Pediatrics 101 (4 Pt 1) (1998) 658–662.
[4] R.P. Batycky, J. Hanes, R. Langer, D.A. Edwards, A theoretical model of erosion and macromolecular drug release from biodegrading microspheres, J. Pharm. Sci. 86 (12) (1997) 1464–1477.
[5] D.S. Kohane, J.Y. Tse, Y. Yeo, R. Padera, M. Shubina, R. Langer, Biodegradable polymeric microspheres and nanospheres for drug delivery in the peritoneum, J. Biomed. Mater. Res., A 77 (2) (2006) 351–361.
[6] C. Raman, C. Berkland, K. Kim, D.W. Pack, Modeling small-molecule release from PLG microspheres: effects of polymer degradation and nonuniform drug distribution, J. Control. Release 103 (1) (2005) 149–158.
[7] C. Berkland, K. Kim, D.W. Pack, PLG microsphere size controls drug release rate through several competing factors, Pharm. Res. 20 (7) (2003) 1055–1062.
[8] C. Berkland, M. King, A. Cox, K. Kim, D. Pack, Precise control of PLG microsphere size provides enhanced control of drug release rate, J. Control. Release 82 (1) (2002) 137–147.
[9] C. Berkland, M. Kipper, K. Kim, B. Narasimhan, D. Pack, Microsphere size, precipitation kinetics, and drug distribution control drug release from biodegradable polyanhydride microspheres, J. Control. Release 94 (1) (2003) 129–141.
[10] S. Suarez, P. O'Hara, M. Kazantseva, C.E. Newcomer, R. Hopfer, D.N. McMurray, A.J. Hickey, Respirable PLGA microspheres containing rifampicin for the treatment of tuberculosis: screening in an infectious disease model, Pharm. Res. 18 (9) (2001) 1315–1319.
[11] L.A. Dailey, N. Jekel, L. Fink, T. Gessler, T. Schmehl, M. Wittmar, T. Kissel, W. Seeger, Investigation of the proinflammatory potential of biodegradable nanoparticle drug delivery systems in the lung, Toxicol. Appl. Pharmacol. 215 (1) (2006) 100–108.
[12] N.Y. Chew, H.K. Chan, Use of solid corrugated particles to enhance powder aerosol performance, Pharm. Res. 18 (11) (2001) 1570–1577.
[13] M. Geiser, N. Leupin, I. Maye, V.I. Hof, P. Gehr, Interaction of fungal spores with the lungs: distribution and retention of inhaled puffball (*Calvatia excipuliformis*) spores, J. Allergy Clin. Immunol. 106 (1 Pt 1) (2000) 92–100.
[14] D.A. Edwards, J. Hanes, G. Caponetti, J. Hrkach, A. Ben-Jebria, M.L. Eskew, J. Mintzes, D. Deaver, N. Lotan, R. Langer, Large porous particles for pulmonary drug delivery, Science 276 (1997) 1868–1871.
[15] J. Fu, J. Fiegel, E. Krauland, J. Hanes, New polymeric carriers for controlled drug delivery following inhalation or injection, Biomaterials 23 (22) (2002) 4425–4433.
[16] C. Dunbar, G. Scheuch, K. Sommerer, M. DeLong, A. Verma, R. Batycky, In vitro and in vivo dose delivery characteristics of large porous particles for inhalation, Int. J. Pharm. 245 (1–2) (2002) 179–189.
[17] R. Vanbever, J.D. Mintzes, J. Wang, J. Nice, D. Chen, R. Batycky, R. Langer, D.A. Edwards, Formulation and physical characterization of large porous particles for inhalation, Pharm. Res. 16 (11) (1999) 1735–1742.
[18] J.B. Lyczak, C.L. Cannon, G.B. Pier, Lung infections associated with cystic fibrosis, Clin. Microbiol. Rev. 15 (2) (2002) 194–222.
[19] C. Berkland, K. Kim, D.W. Pack, Fabrication of PLG microspheres with precisely controlled and monodisperse size distributions, J. Control. Release 73 (1) (2001) 59–74.
[20] C. Berkland, E. Pollauf, D.W. Pack, K.K. Kim, Uniform double-walled polymer microspheres of controllable shell thickness, J. Control. Release 96 (1) (2004) 101–111.
[21] C. Berkland, E. Pollauf, C. Raman, R. Silverman, K.K. Kim, D.W. Pack, Macromolecule release from monodisperse PLG microspheres: control of release rates and investigation of release mechanism, J. Pharm. Sci. 96 (5) (2007) 1176–1191.
[22] C. Berkland, E. Pollauf, N. Varde, D.W. Pack, K.K. Kim, Monodisperse liquid-filled biodegradable microcapsules, Pharm. Res. 24 (5) (2007) 1007–1013.
[23] C.J. Tsai, H.M. Chein, S.T. Chang, J.Y. Kuo, Performance evaluation of an API aerosizer, J. Aerosol Sci. 29 (7) (1998) 839–853.
[24] O.B. Peersen, X. Wu, I. Kustanovich, S.O. Smith, Variable-amplitude cross-polarization MAS NMR, J. Magn. Reson., Ser. A 104 (3) (1993) 334–339.
[25] E.O. Stejskal, J. Schaefer, J.S. Waugh, Magic-angle spinning and polarization transfer in proton-enhanced NMR, J. Magn. Reson. (1969) 28 (1) (1977) 105–112.
[26] A.E. Bennett, C.M. Rienstra, M. Auger, K.V. Lakshmi, R.G. Griffin, Heteronuclear decoupling in rotating solids, J. Chem. Phys. 103 (16) (1995) 6951–6958.
[27] D.H. Barich, E.M. Gorman, M.T. Zell, E.J. Munson, 3-Methylglutaric acid as a ^{13}C solid-state NMR standard, Solid State Nucl. Magn. Reson. 30 (3–4) (2006) 125–129.
[28] G. Metz, X. Wu, S.O. Smith, Ramped-amplitude cross polarization in magic-angle-spinning NMR, J. Magn. Reson., Ser. A 110 (2) (1994) 219–227.
[29] W.I. Li, K.W. Anderson, R.C. Mehta, P.P. DeLuca, Prediction of solvent removal profile and effect on properties for peptide-loaded PLGA microspheres prepared by solvent extraction/evaporation method, J. Control. Release 37 (3) (1995) 199–214.
[30] K.J. Pekarek, J.S. Jacob, E. Mathiowitz, Double-walled polymer microspheres for controlled drug release, Nature 367 (1994) 258–260.
[31] K.J. Pekarek, J.S. Jacob, E. Mathiowitz, One-step preparation of double-walled microspheres, Adv. Mater. 6 (1994) 684–687.
[32] E.J. Pollauf, C. Berkland, K.K. Kim, D.W. Pack, In vitro degradation of polyanhydride/polyester core-shell double-wall microspheres, Int. J. Pharm. 301 (1–2) (2005) 294–303.
[33] R.B. Bird, W.E. Stewart, E.N. Lightfoot, Transport Phenomena, 2nd Edition. Wiley Press, 2001.
[34] D.A. Edwards, A. Ben-Jebria, R. Langer, Recent advances in pulmonary drug delivery using large, porous inhaled particles, J. Appl. Physiol. 85 (2) (1998) 379–385.